Electrical and Computer Engineering Publications   Dept. of Electrical and Computer Engineering

2012

Impact of active layer design on InGaN radiative recombination coefficient and LED performance

X. Li
Virginia Commonwealth University

S. Okur
Virginia Commonwealth University, okurs@vcu.edu

F. Zhang
Virginia Commonwealth University

See next page for additional authors

Authors

X. Li, S. Okur, F. Zhang, V. Avrutin, Ü. Özgür, H. Morkoç, S. M. Hong, S. H. Yen, T. C. Hsu, and A. Matulionis

Impact of active layer design on InGaN radiative recombination coefficient and LED performance

X. Li,[1,a] S. Okur,[1] F. Zhang,[1] V. Avrutin,[1] Ü. Özgür,[1] H. Morkoç,[1] S. M. Hong,[2] S. H. Yen,[2] T. C. Hsu,[2] and A. Matulionis[3]

[1]*Department of Electrical and Computer Engineering, Virginia Commonwealth University, Richmond, Virginia 23284, USA*
[2]*EPISTAR Corporation, Hsinchu 300, Taiwan*
[3]*Semiconductor Physics Institute of Center for Physical Science and Technology, Vilnius, Lithuania*

The relative roles of radiative and nonradiative processes and the polarization field on the light emission from blue (∼425 nm) InGaN light emitting diodes (LEDs) have been studied. Single and multiple double heterostructure (DH) designs have been investigated with multiple DH structures showing improved efficiencies. Experimental results supported by numerical simulations of injection dependent electron and hole wavefunction overlap and the corresponding radiative recombination coefficients suggest that increasing the effective active region thickness by employing multiple InGaN DH structures separated by thin and low barriers is promising for LEDs with high efficiency retention at high injection. The use of thin and low barriers is crucial to enhance carrier transport across the active region. Although increasing the single DH thickness from 3 to 6 nm improves the peak external quantum efficiency (EQE) by nearly 3.6 times due to increased density of states and increased emitting volume, the internal quantum efficiency (IQE) suffers a loss of nearly 30%. A further increase in the DH thickness to 9 and 11 nm results in a significantly slower rate of increase of EQE with current injection and lower peak EQE values presumably due to degradation of the InGaN material quality and reduced electron-hole spatial overlap. Increasing the number of 3 nm DH active regions separated by thin (3 nm) $In_{0.06}Ga_{0.94}N$ barriers improves EQE, while maintaining high IQE (above 95% at a carrier concentration of 10^{18} cm^{-3}) and showing negligible EQE degradation up to 550 A/cm^2 in 400×400 μm^2 devices due to increased emitting volume and high radiative recombination coefficients and high IQE. Time-resolved photoluminescence measurements revealed higher radiative recombination rates with increasing excitation due to screening of the internal field and enhanced electron and hole overlap at higher injection levels. To shed light on the experimental observations, the effect of free-carrier screening on the polarization field at different injection levels and the resulting impact on the quantum efficiency were investigated by numerical simulations. © 2012 American Institute of Physics. [http://dx.doi.org/10.1063/1.3699199]

I. INTRODUCTION

InGaN-based light-emitting diodes (LEDs) enabled a wide range of applications including full-color displays, back-lighting sources for displays, and general lighting.[1] The applications of LEDs, particularly for general lighting utilizing white LEDs, require further improvements in device performance.[2] As LED technology matures, it is highly desirable for LEDs to emit a high luminous flux while retaining high quantum efficiencies at high injection levels. However, typical state-of-the-art multiple quantum well (MQW) InGaN-based LEDs demonstrate maximum quantum efficiency at a drive current density as low as 10 A/cm^2 in some reported cases, which degrades to as little as half of its maximum value at current densities above 100 A/cm^2. To retain the quantum efficiency at high current levels a straightforward approach would be to increase the number of quantum wells (QWs) in the active region. However, due to the poor hole transport, light is emitted mainly from the QWs closest

to the *p*-GaN in typical *c*-plane InGaN/GaN LEDs.[3–5] An alternative approach is to utilize double heterostructure (DH) active regions ensuring uniform carrier spreading across the active region.[6] Among the ramifications of DH are the loss of InGaN quality and the increased band bending due to the polarization field. In spite of this, Li *et al.*[7] have demonstrated 9 nm InGaN-based single DH LEDs exhibiting peak external quantum efficiency (EQE) approximately 25% higher than that of a MQW-LED [6 period $In_{0.15}Ga_{0.85}N$ (2 nm)/$In_{0.06}Ga_{0.94}N$(3 nm)] with low efficiency degradation (∼10%) up to current densities of 600 A/cm^2. As expected, at low injection levels, i.e., below 60 A/cm^2, the 9 nm DH-LEDs exhibit a relatively slower EQE rate of increase with injection current compared to that of the MQW-LED. This observation is consistent with the internal quantum efficiency (IQE) measurements we performed, and is caused by the larger spatial separation of electrons and holes owing to the stronger effect of the polarization field in thicker active regions. Essentially this is equivalent to a radiative recombination coefficient which increases with injection current before other ailments set in.

[a]Electronic mail: xli.vcu@gmail.com.

Very few studies have been carried out on the quantum efficiency of InGaN-based DH structures.[6–8] In this work, we report that with increasing DH active layer thickness from 3 to 6 nm the relative EQE increased considerably despite reduction in IQE and the rate of increase of efficiencies with increasing injection. The relative EQE was enhanced substantially in dual 3 nm DH and dual 6 nm DH LEDs, separated by a 3 nm-thick $In_{0.06}Ga_{0.94}N$ barrier. Incorporating more DH active regions of the same thickness, separated by thin and low InGaN barriers, results in enhanced emission intensity without any discernible degradation of the active region quality unlike that observed in thicker single DH layers due to strain relaxation with increasing InGaN thickness. We find that employment of low and thin InGaN barriers is essential for ameliorating carrier (particularly hole) transport across the active region. Numerical simulations and time-resolved photoluminescence (TRPL) measurements elucidated carrier injection effects on the optical transition energy and the overlap of the electron and hole spatial distributions.

II. EXPERIMENTAL DETAILS

The *c*-plane InGaN LED structures, emitting at ~425 nm, were grown on ~3.7 μm-thick *n*-type GaN templates on sapphire in a vertical low-pressure metalorganic chemical vapor deposition (MOCVD) system. The active regions contained either one or more (dual, quad, hex) $In_{0.15}Ga_{0.85}N$ DH active regions separated by 3 nm $In_{0.06}Ga_{0.94}N$ barriers. Fig. 1 shows the conduction band diagram for dual DH structures where flat bands are shown for simplicity. All the structures incorporate a staircase electron injector (SEI) layer for efficient thermalization of hot carriers prior to injection into the active region, and a 60 nm Si-doped (2×10^{18} cm^{-3}) $In_{0.01}Ga_{0.99}N$ underlying layer for improving the quality of overgrown layers. The SEI consists of two 5 nm InGaN layers (two-layer SEI) with step-increased In compositions of 4% and 8%, inserted in the given order below the active region. A continuously graded InGaN structure, which is a very efficient electron cooler, can be used as the electron injector as well. The SEI steps have conduction band potential energy drop equal to or more than one LO phonon energy (92 meV for GaN) and enhanced electron thermalization through LO phonon emission. The LED structures were completed with 100 nm thick Mg-doped *p*-GaN layers having 4×10^{17}/cm^3 hole density, as determined by Hall measurements on a separate
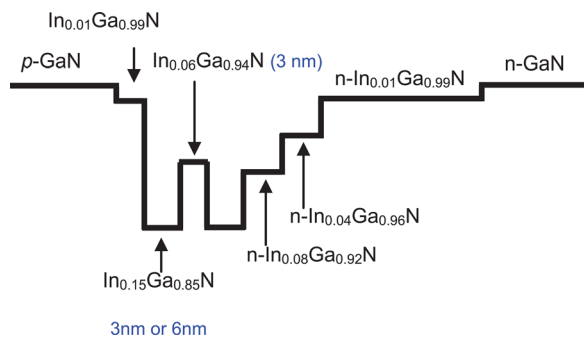
calibration sample. For devices, square mesa patterns (400×400 μm^2) were formed by conventional lithography and chlorine-based inductively coupled plasma (ICP) etching. Ti/Al/Ni/Au (30/100/40/50 nm) metallization annealed at 800 °C for 60 s was used for *n*-type ohmic contacts, and 5 nm/5 nm Ni/Au electrodes served as the semi-transparent *p*-contact. Finally, 40/50 nm Ni/Au electrodes were deposited on part of the mesas for contact pads.

III. RESULTS AND DISCUSSION

IQE and EQE values for all LED structures were measured at different injection levels and the effects of the active region design and the resulting polarization fields and band structures were investigated. For determination of the IQE from optical measurements, injection dependent radiative recombination coefficients obtained from numerical simulations of the band structures and electron and hole distributions were used. IQE values and the effects of the polarization fields were also deduced from excitation density dependent measurements of recombination dynamics.

A. IQE of single and multi active layer DH structures

In the realm of Fermi's Golden Rule, the spontaneous transition rate from a group of initial states *i* in the conduction band to a group of final states *f* in the valence band separated by a transition energy $\hbar\omega$ can be expressed as

$$T_{i \to f} = \frac{2\pi}{\hbar} |H_{fi}|^2 \rho_r(\hbar\omega) F(\hbar\omega), \quad (1)$$

where $\rho_r(\hbar\omega)$ is the reduced density of states, $\hbar\omega$ is the transition energy, $F = f_c(1 - f_v)$ is the Fermi factor given in terms of the Fermi functions for the conduction (f_c) and valence bands (f_v), and H_{fi} is the transition matrix element given by

$$H_{fi} = \langle \Psi_f | H | \Psi_i \rangle = \int \Psi_f^*(\mathbf{r}) H(\mathbf{r}) \Psi_i(\mathbf{r}) d^3\mathbf{r}. \quad (2)$$

For a system with confinement along the *z*-direction (growth direction), the wavefunctions can be expressed using the envelope functions as $\Psi(\mathbf{r}) = \psi(z)\phi(\mathbf{r}_{xy})$. If the physical interaction operator is independent of the variable *z*, the matrix element can be simplified to[9]

$$H_{fi} = \left(\frac{eA_0}{2m_0}\right) M \int \psi_f^*(z)\psi_i(z)dz, \quad (3)$$

where A_0 is the magnitude of the sinusoidal local vector potential, *e* is the electron charge, m_0 is the free electron mass, and *M* is the in-plane momentum matrix element. The spontaneous transition rate in Eq. (1) can then be written as

$$T_{i \to f} = \frac{2\pi}{\hbar} \left(\frac{eA_0}{2m_0}\right)^2 |M|^2 |\int \psi_f^*(z)\psi_i(z)dz|^2 \rho_r(\hbar\omega) F(\hbar\omega). \quad (4)$$

Equation (4) indicates that a necessary condition for efficient recombination is the spatial overlap between the electron and hole wavefunctions (ψ_e and ψ_h) and the radiative

FIG. 1. Conduction band diagram for dual DH LED structures.

The labels in the figure: $In_{0.01}Ga_{0.99}N$; *p*-GaN; $In_{0.06}Ga_{0.94}N$ (3 nm); n-$In_{0.01}Ga_{0.99}N$; n-GaN; n-$In_{0.04}Ga_{0.96}N$; n-$In_{0.08}Ga_{0.92}N$; $In_{0.15}Ga_{0.85}N$; 3nm or 6nm

recombination rate is proportional to the squared overlap integral when electrons and holes are confined in the *z*-direction.

For quantum-confined structures it has been suggested that low-dimensional equivalents of the bimolecular radiative recombination *B* coefficient should be introduced to eliminate the artificial dependence of the radiative recombination current on size, such as the active region width in two-dimensional (2D) systems.[9] For InGaN quantum wells with confinement along the *z*-direction, defining the spontaneous transition rate as $T_{spont} = B_{2D}n_{2D}p_{2D}$, where n_{2D} and p_{2D} are the 2D electron and hole densities, respectively. The 2D *B* coefficient can be expressed in terms of the momentum matrix element in Eq. (4)[9]

$$B_{2D} = \frac{4\pi n\hbar^2}{\varepsilon_0 c^3 k_B T} \frac{(\hbar\omega)}{m_e^* m_h^*} \left(\frac{e}{2m_0}\right)^2$$
$$\times |M|^2 \left|\int_0^\infty \psi_h^*(z)\psi_e(z)dz\right|^2 \rho_r(\hbar\omega), \quad (5)$$

where *n* is the refractive index, ε_0 is the permittivity of free space, *c* is the speed of light, $\hbar\omega$ is photon energy, $k_B T$ is the thermal energy, and m_e^* and m_h^* are the electron and hole effective masses (obtained using linear interpolation from the binary values for a given In content), respectively. The momentum matrix element *M* can be obtained from the in-plane interband transition matrix element (for polarization within the plane), $P_{cv} = 2|M|$,[10] which has been determined from the absorption measurements for binaries InN and GaN.[11] Using a value of $P_{cv} = 9.6 \times 10^{-20}$ g cm/s obtained from linear interpolation for the required composition, the B_{2D} coefficient was calculated to be 1.8×10^{-4} cm^2 s^{-1} for an In$_{0.15}$Ga$_{0.85}$N active region assuming full overlap of electron and hole wavefunctions. In order to make the transition from the 2D to the 3D case to be able to employ the conventional 3D rate equation, the 2D *B* coefficient should be multiplied by the active region thickness, L_z. To test this

approach and the validity of the 2D approximation, the 3D limit for the *B* coefficient for In$_{0.15}$Ga$_{0.85}$N was also calculated from[12]

$$B_{3D} = \frac{e^2 n}{m_0^2 c^3 \hbar^2} \left(\frac{2\pi\hbar^2}{k_B T}\right)^{3/2} \times M^2 \times \frac{1}{(\bar{m}_x \bar{m}_y \bar{m}_z)^{1/2}} \hbar\omega, \quad (6)$$

where $\bar{m}_{x,y,z} = m_{e(x,y,z)} + m_{h(x,y,z)}$. The 3D *B* coefficient calculated using Eq. (6) is 5×10^{-11} cm^3 s^{-1} for In$_{0.15}$Ga$_{0.85}$N. This value is smaller than that obtained using $B_{2D}L_z$ even for the thinnest active region investigated in this study with L_z = 3 nm. Therefore, we assume that all the LED structures employed here exhibit 3D behavior but with an electric field along the growth direction reducing the spatial overlap of charge carriers in the active region. Consequently, the injection dependent overlap integral of the electron and hole wavefunctions should be incorporated into the calculation of the 3D *B* coefficients using the upper limit for full overlap, 5×10^{-11} cm^3/s

$$B = (5 \times 10^{-11})[\text{cm}^3\text{s}^{-1}] \times \left|\int_0^\infty \psi_h^*(z)\psi_e(z)dz\right|^2. \quad (7)$$

In this study, the effects of the active region design and the resulting polarization-induced field[13] on the overlap integral and the associated spontaneous recombination rates were investigated at different injection levels. Fig. 2(a) presents the simulated bimolecular recombination coefficients, *B*, which are obtained from the transition matrix element, and thus the simulated squared overlap integrals of the electron and hole wavefunctions within the DH active regions. It should be mentioned that the calculated *B* coefficients may vary slightly based on the material parameters used for a given structure; however, this would not affect the overall conclusions of this paper. The calculated *B* coefficients are also plotted in Fig. 2(b) as a function of supplied electrical power per unit cross-sectional area, which is the product of injection current density and applied voltage used in the
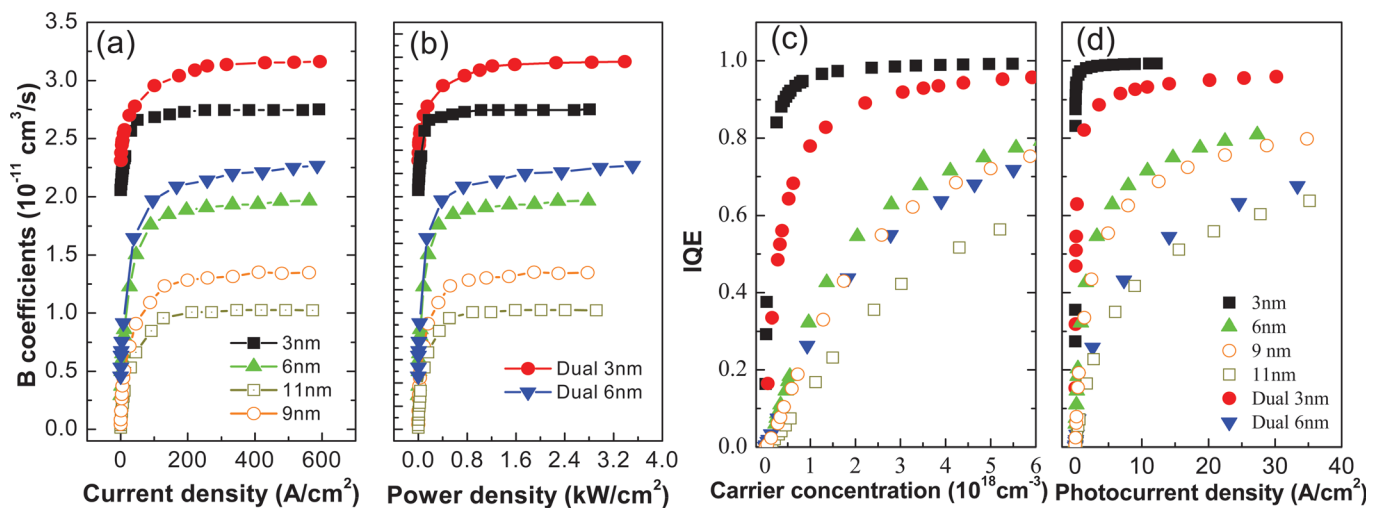

FIG. 2. Calculated *B* coefficients using squared overlap integrals of electron and hole wavefunctions (proportional to radiative recombination rate) within the active region as a function of (a) current density calculated using Silvaco ATLAS simulations and (b) injection electrical power density (the product of applied voltages and current densities). (c) IQE values determined from excitation-dependent PL for LEDs with various DH thickness by using injection dependent *B* coefficients from (a). (d) IQE values vs photocurrent density converted from carrier concentration using Eq. (8).

simulations. It is apparent from Fig. 2(a) that the B coefficient, instead of being constant as assumed in Ref. 15, depends on the injection current density for a given design,[14] increasing with injection due to screening of the internal fields by free carriers. Naturally, the B coefficient tends to saturate at high injection levels as the nearly flatband condition is approached.[13] It is also evident that thinner active layers have relatively larger spatial overlap of the electron and hole wavefunctions. The single 3 nm DH LED shows a 30% higher squared overlap integral value compared to the single 6 nm DH LED at a current density of $\sim$300 A/cm^2. The lower B coefficients in wider active regions are attributed to the increased spatial separation of electrons and holes by the larger contribution of the polarization fields. Moreover, while the dual and single DH structures exhibit comparable overlap integrals at low injection levels (below 100 A/cm^2), the dual DH structures surpass their single DH counterparts as the injection current increases. For example, the dual 3 nm DH LEDs show 15% higher EQEs compared to the single 3 nm DH LEDs at a current density of 500 A/cm^2. Furthermore, the rate of increase for the B coefficient versus the current density at low injection levels is reduced with increasing active layer thickness, which is consistent with the experimental IQE and EQE data shown in Fig. 2(c) and Fig. 3, respectively.

The room temperature IQE values were measured by resonant optical excitation intensity-dependent photoluminescence (PL),[15] but with invoking injection dependent B coefficients to produce more accurate IQE values versus the photoinduced carrier concentration. The generation rates in optical excitation were matched to those calculated from the electrical injection power density used in the simulations to account for the carrier density (injection) dependence of the B coefficients. The excitation wavelength from a frequency doubled Ti:Sapphire laser was set to 385 nm for photogeneration of carriers inside the active region only.[16,17] Fig. 2(c) shows the resulting IQE values versus the carrier concentration for all the DH structures. The IQE for a single

3 nm DH LED reaches above 95% at a carrier concentration of 10^{18} cm^{-3}, which corresponds to a photocurrent density of 1 A/cm^2 as indicated in Fig. 2(d). The photocurrent densities in Fig. 2(d) are obtained from carrier densities using the rate equation (as resonant excitation ensures no carrier leakage)[7]

$$G = J/J(qd)(qd) = An + Bn^2 + Cn^3$$
$$\eta_{IQE} = \frac{Bn^2}{G}, \qquad (8)$$

where G is the generation rate, n is the carrier density, q is the electron charge, d is the thickness of the active layer, J is the photocurrent density, and η_{IQE} is the IQE. The terms A and B represent Shockley-Read-Hall (SRH) nonradiative recombination and radiative recombination coefficients, respectively. The Auger coefficient C, which we deem small,[2] is neglected, and the A coefficient is obtained from the fitting ($\sim$10^5-10^7 /s). As can be seen, when we insert a second DH active region separated by a 3 nm thick In$_{0.06}$Ga$_{0.94}$N barrier, which still allows efficient hole transport,[7] the IQE rate of increase with photocurrent density is slower than that for the single 3 nm DH, and a 90% IQE is reached at a photocurrent density of $\sim$5 A/cm^2 compared to 0.3 A/cm^2 in the single 3 nm DH. However, the IQE values are very similar for both structures at high injection levels. Increasing the DH thickness to 6 and 9 nm reduces IQE and its rate of increase substantially. As shown in Fig. 2(c), IQEs for both 6 and 9 nm DH LEDs increase relatively slowly with carrier concentration and reach 70% at around a carrier density of 4×10^{18} cm^{-3}. The dual 6 nm DH essentially has quite a similar IQE dependence on carrier concentration as the single 6 nm DH, as shown in Fig. 2(c), whereas the dependence on photocurrent density shows an apparent discrepancy due to increased overall active region thickness (12 nm) and larger B coefficients used in the conversion calculation from density of photocarriers to photocurrent density (see Eq. (8)). With increasing DH thickness, the IQE values degrade and the IQE rate of increase with the carrier concentration becomes slower, the most severely for DH thickness of 11 nm. These effects in wider active regions can be partially attributed to the stronger polarization field effects and decreased electron and hole wavefunction overlap and partially to the degraded layer quality with increasing InGaN thickness, which will increase nonradiative recombination.

B. EQE of single and multi active layer DH structures

As mentioned previously, uniform electron and hole generation in the active region can be achieved under resonant optical excitation, which prevents carrier overflow induced efficiency degradation observed under electrical injection. Therefore, LEDs exhibiting the highest IQE values may not necessarily display the highest EQE values due to possible electron leakage. To determine the relative EQE, on-wafer pulsed electroluminescence (EL) measurements were carried out for all the investigated LEDs with no particular effort to enhance light extraction. Care was taken to assure the same light collection geometry among all the chips tested. To
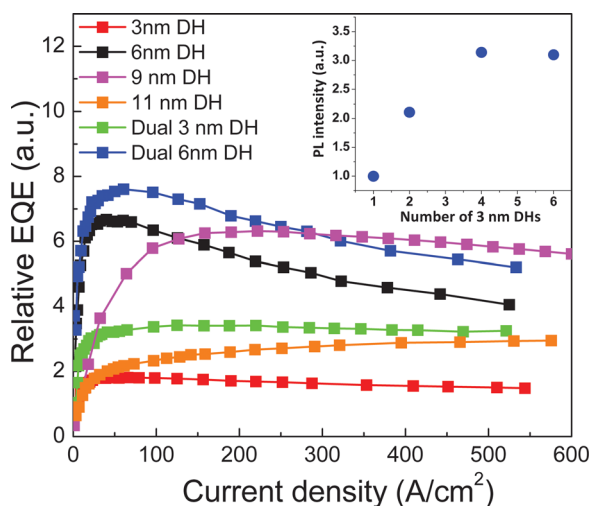

FIG. 3. Relative external quantum efficiencies of DH LEDs as a function of pulsed injection current density (0.1% duty cycle and 1 kHz frequency). The inset shows the normalized resonant PL intensity vs the number of 3 nm DH active regions.

achieve the same light outcoupling efficiency, the same *p*-GaN growth conditions were used and all samples were fabricated together in one run. Moreover, the light emission intensity showed less than 5% variation among at least five devices measured on the same wafer. Note that not all the light emanating from the LED was collected. Fig. 3 shows the relative EQE values for the LED structures with various DH thicknesses.

As presented in Figs. 2(c) and 2(d), the 3 nm DH exhibits the highest IQE, reaching 97.5% at a low carrier level $\sim10^{18}$ cm^{-3} (corresponding to 1 A/cm^2). Its EQE also increases at a fast rate with current injection and reaches its maximum at $\sim$30 A/cm^2 owing to the greater spatial overlap of electron and hole wavefunctions. However, the overall EQE is only 23% that of the single 6 nm DH LED, likely due to lower density of states within the 3 nm InGaN active layer (nearly two-dimensional states) as compared to 6 nm InGaN layer (nearly three-dimensional states) as well as the smaller active layer volume and thus smaller overall carrier density. Noticeably, when another 3 nm In$_{0.15}$Ga$_{0.85}$N layer separated by a 3 nm In$_{0.06}$Ga$_{0.94}$N barrier is added to the active region, the EQE value is doubled due to increased active layer volume, which is consistent with resonant PL measurements showing a twofold increase in emission intensity for the same excitation power (see the inset of Fig. 3).

The single 6 nm DH LED structure shows the maximum relative EQE values at current density $\sim$41 A/cm^2, slightly higher than that for the 3 nm DH LEDs, indicative of a slower rate of increase with injection for the 6 nm DH LED. However, it suffers from a large efficiency droop (reduced by 38% at 550 A/cm^2 with respect to the maxima) with increasing current density. The dual 6 nm DH LED shows $\sim$12% higher peak EQE values and less efficiency droop percentile (reduced by $\sim$30%) under the same current density. This implies that the layer quality for dual 6 nm DH is inferior to the single 6 nm DH, unlike in the 3 nm DH case, which showed doubled EQE values when the dual active regions separated by a thin barrier were used. Increasing the individual layer thickness further to 9 and 11 nm results in deteriorated layer quality and the 11 nm single DH LED exhibits much lower EQE values. We should also note that the dual 6 nm DH shows 20% higher peak EQE than that obtained from the single 9 nm DH and a much faster increasing rate of EQE with current injection. It is also observed that the 9 nm DH LED exhibits lower EQE values at lower injection levels (less than 125 A/cm^2) due to a much slower rise of EQE with injection although its EQE saturates at higher values with increasing injection level. At high current densities, e.g., 550 A/cm^2, the 9 nm single DH shows 15% and 32% higher EQE than those for dual 6 nm and single 6 nm DH LEDs, respectively, due to greater efficiency reduction in single and dual 6 nm DHs. Specifics of the degradation mechanisms and methods to mitigate them are still under investigation.

Promisingly, the EQEs for the single 3 nm and dual 3 nm DH LEDs show negligible degradation with increasing injection current density up to 600 A/cm^2. According to the IQE and relative EQE data for single 3 nm and dual 3 nm DH LEDs, there seems to be a trade-off to achieve both high IQE and EQE in *c*-plane InGaN DH LEDs. However, the negligi-

ble droop and rapid initial increase of quantum efficiencies with injection current in single 3 nm and dual 3 nm DH LEDs are critical to InGaN LED improvement. In an effort to enhance the relative EQE of such DH structures further we have grown LED structures with more (4 and 6) 3 nm thick active regions separated by the thin In$_{0.06}$Ga$_{0.94}$N barriers. Resonant PL measurements revealed that the PL intensity of quad 3 nm DH LED is nearly 4 times higher than that for single 3 nm DH; however, the PL intensity of the hex 3 nm DH LED did not scale to 6 times that from the single 3 nm DH but is very close to that from the quad 3 nm DH LED, which is shown in the inset of Fig. 3. This behavior can be attributed to the relaxation of the active regions upon increasing the number of 3 nm DH layers beyond four. The particular processes for the above observations are discussed below.

In biaxially strained InGaN/GaN layers, the mismatch strain induces a polarization field (allowed by the wurtzite-structure lattice symmetry) along the growth direction.[18] This strain induced piezoelectric field and spontaneous polarization field tilts the potential profile, resulting in triangular quantum wells in the hetero-interfaces of active regions, as shown in the simulated conduction and valence band edges of Fig. 4(a) at an injected current density of 1100 A/cm^2
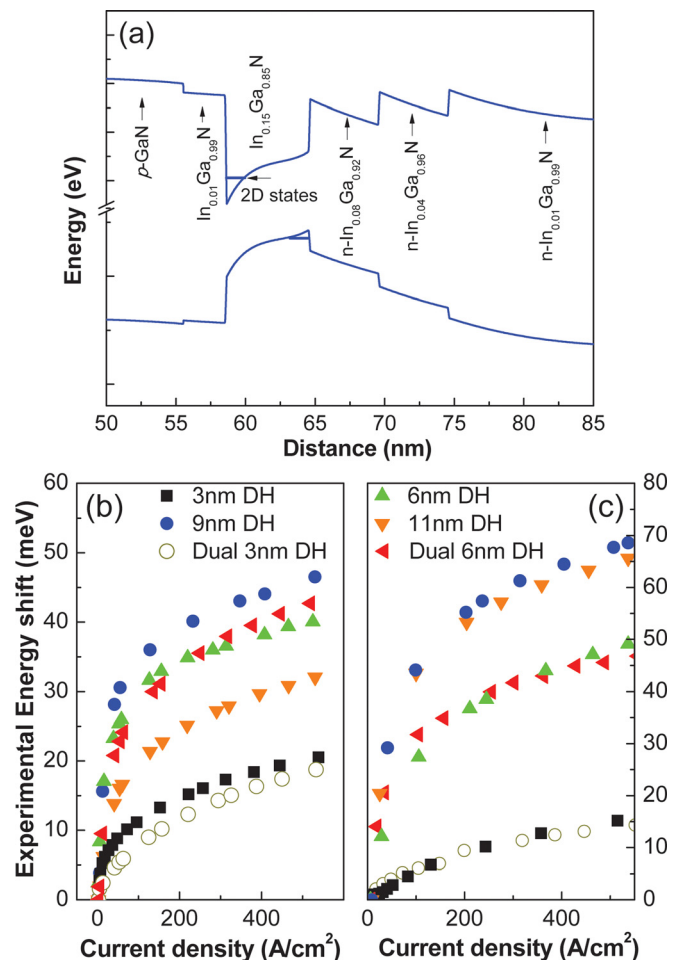

FIG. 4. (a) Energy band edge profiles simulated at 3.16 V forward bias (corresponding to 1100 A/cm^2); (b) peak emission energy shift as a function of injection current density from EL measurements; (c) peak emission energy shift as a function of injection current density from Silvaco simulations for the 6 nm DH structure.

using the commercial Silvaco ATLAS software package. Consequently, the optical transition energy is reduced. Therefore, with increasing current injection, a blueshift will occur and the magnitude of the blueshift depends on the active layer thickness.[19] Fig. 4(b) shows the observed peak emission energy shift as a function of injection current density from EL measurements. Upon current injection, the polarization fields in the strained InGaN DH layer are screened by free carriers, which weakens the quantum confined Stark effect (QCSE), and then increases the transition energy resulting in the blueshift in emission. Larger peak energy shifts were observed with injection when the DH thickness is increased from 3 to 9 nm, as presented in Fig. 4(b). However, increasing DH thickness further to 11 nm reduced the shift substantially, most probably due to partial relaxation of the InGaN active layer, which is not considered in the simulation software.

Similar to our earlier observations,[7] a large portion of the energy shift occurs at low injection levels (<50 A/cm^2) followed by a slower shift with further increase in injection. This is attributed to the presence of triangular potential wells at the interfaces, which are filled rather rapidly even at relatively low injection levels causing the large initial blueshift. Recombination from the higher lying quasi-continuum states and 3D states in the DH active region start to contribute to emission with increased injection, resulting in the slower blueshift observed.

For single 6 nm, dual 6 nm, and single 9 nm DH LEDs, a significant 25 meV energy shift was observed with an initial increase of current density to 40 A/cm^2, while only a 8 meV shift is evident for the 3 nm DH LED within the same current density range. Fig. 4(c) shows the simulated peak energy shift as a function of current density obtained using Silvaco ATLAS. The polarization charge densities of 7.7×10^{12} cm^{-2} and 3.8×10^{12} cm^{-2} have been used for the interfaces between the In$_{0.01}$Ga$_{0.99}$N barrier and the In$_{0.15}$Ga$_{0.85}$N active layer, and the In$_{0.15}$Ga$_{0.85}$N active layer and the In$_{0.08}$Ga$_{0.92}$N SEI, respectively, which are within the range of reported values[20] and provide energy shifts in the range comparable to those observed experimentally [Fig. 4(b)]. The tendency is consistent with the experimental results except for the 11 nm DH structure. The simulated peak energy shift dependence on injection for the 11 nm DH LED is very similar to that of the 9 nm DH structure, as with increasing DH thickness the band profiles become similar. As alluded to earlier, the observed discrepancy in the experimental data, however, is likely due to the strain-driven material quality degradation for 11 nm DH neglected in simulations. We should also note that varying the polarization charge in the simulations changes the absolute energy shift, but does not affect the peak energy shift dependence on the active layer thickness.

C. IQE of DH structures from recombination dynamics

In order to better understand the recombination dynamics for DH LEDs, excitation density dependent TRPL measurements were performed using 385 nm wavelength excitation from a frequency-doubled Ti:Sapphire laser. The

photoluminescence was collected using an optical fiber and focused into a spectrometer attached to a 30 ps resolution Hamamatsu streak camera. Fig. 5 shows TRPL data for the 3 nm, dual 3 nm, 6 nm, and dual 6 nm DH LEDs at different excitation power densities: 0.08, 0.20, and 1.25 kW/cm^2. All of the DH LED structures investigated here (9 and 11 nm DH not shown) exhibit similar excitation intensity dependence behavior. The analysis of transient PL in a variety of InGaN heterostructures, single quantum wells,[21] multiple quantum wells,[22] and double heterostructures,[23] have been performed using multiple[24] or stretched exponential[25] decay functions representing different radiative and nonradiative relaxation pathways. In a recent study, Kim *et al.*[26] proposed a method by which the radiative and nonradiative decay times and IQE values can be deduced from the TRPL data. The transients were fitted using biexponential decays $A_1 e^{-t/\tau_i} + A_2 e^{-t/\tau_f}$, where the fast and slow decay components are represented using initial (τ_i) and final (τ_f) decay times, respectively. Based on the carrier rate equation,[26] radiative and nonradiative decay times can be approximately estimated using $\tau_R \approx 2\tau_i\tau_f/(\tau_f - \tau_i)$ and $\tau_{NR} \approx 2\tau_f$, respectively. The initial (fast) decay of the TRPL spectrum is influenced by both radiative and nonradiative recombination rates, whereas the final (slow) decay is only dependent on nonradiative recombination.

The corresponding radiative and nonradiative decay times extracted from the biexponential fits to the TRPL data from the LEDs investigated here are listed in Table I. As shown in Fig. 5, the initial decay time has a strong dependence on optical excitation power density, decreasing with increasing power, while the final decay time remains nearly constant for the range of excitation power densities used.
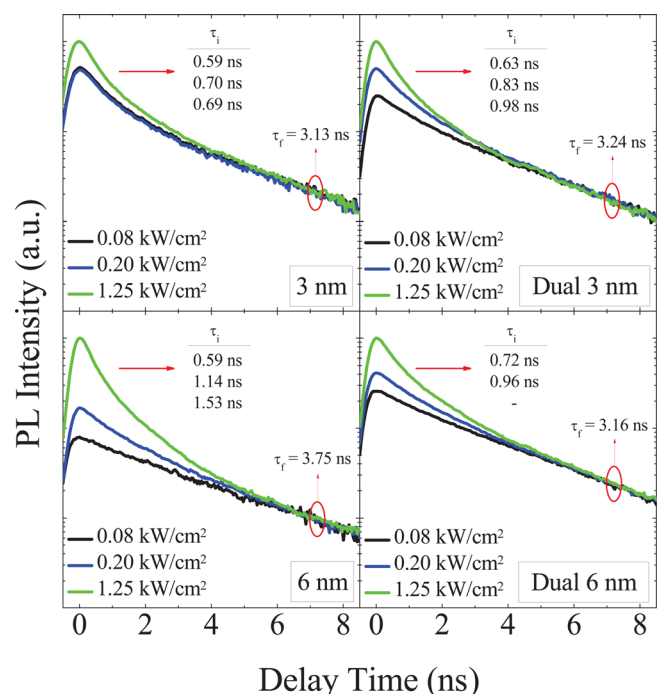

FIG. 5. TRPL results for 3 nm, dual 3 nm, 6 nm, and dual 6 nm DH LEDs for different excitation power densities, 0.08, 0.20, and 1.25 kW/cm^2. TRPL data are fitted with biexponential decay functions $A_1 e^{-t/\tau_i} + A_2 e^{-t/\tau_f}$ to find initial (τ_i) and final (τ_f) decay times, which are also indicated.

TABLE I. The radiative and nonradiative decay times and amplitude ratios extracted from the fitted biexponential decay parameters and IQE values for the 3 nm, dual 3 nm, 6 nm, dual 6 nm, and 11 nm DH LED structures.

DH LED	τ_R[ns]	τ_{NR}[ns]	$\frac{A_1}{A_2}$	IQE (from Fig. 2)	IQE (from TRPL using the approach in Ref. 26)
0.08 kW/cm^2 excitation power density					
3 nm	1.77	6.26	1.84	0.96	0.78
Dual 3 nm	2.81	6.48	0.70	0.76	0.70
6 nm	5.16	7.50	0.22	0.31	0.59
Dual 6 nm	–	6.32	–	0.18	–
11 nm	–	5.86	–	0.15	–
0.20 kW/cm^2 excitation power density					
3 nm	1.80	6.26	1.83	0.97	0.78
Dual 3 nm	2.23	6.48	2.09	0.84	0.74
6 nm	3.28	7.50	1.57	0.46	0.70
Dual 6 nm	2.76	6.32	0.88	0.32	0.70
11 nm	3.32	5.86	1.37	0.27	0.64
1.25 kW/cm^2 excitation power density					
3 nm	1.45	6.26	3.82	0.99	0.81
Dual 3 nm	1.56	6.48	5.04	0.93	0.81
6 nm	1.40	7.50	9.68	0.72	0.84
Dual 6 nm	1.86	6.32	3.03	0.62	0.77
11 nm	1.67	5.86	9.71	0.57	0.78

The decrease of radiative recombination time, τ_R, with increasing excitation power density is attributed to increased electron and hole wavefunction overlap resulting in efficient radiative recombination, which correlates well with the simulation results presented in Fig. 2(a) and is consistent with earlier observations in single InGaN quantum wells.[27] Furthermore, the final decay rate, which depends on the nonradiative recombination only, is excitation intensity independent as the nonradiative recombination centers are fully saturated at high excitation power densities. In addition, as can be seen from the increasing amplitude fractions (A$_1$/A$_2$) of the initial and final decay components with increasing excitation density, the contribution of radiative recombination to carrier decay is larger at higher excitation power densities. The 3 nm and dual 3 nm DH LEDs exhibit faster radiative decays than the other LEDs due to better electron and hole wavefunction overlap, which is consistent with the IQE measurements and the simulation results discussed above (see Fig. 2). Also, the initial PL decays at lowest excitation density for 3 nm and dual 3 nm DHs are more apparent compared to those of other DH LEDs even at low excitation densities, indicating a higher radiative efficiency (Fig. 5).

The IQE values calculated from the measured radiative and nonradiative decay constants using $\eta_{\text{int}} = \tau_{NR}/(\tau_{NR} - \tau_R)$ (Ref. 26) are also listed in Table I. Although these IQE values differ from those shown in Fig. 2 obtained using optical excitation intensity dependent PL measurements (values at the same carrier densities are compared in Table I), they show the same tendency with increasing DH thickness. The differences between the two sets of IQE values are most likely due to the inaccuracy of the materials parameters used, particularly the absolute values of the B coefficients obtained from simulations, which neglect any strain relaxation and material degradation with increasing InGaN thickness, and the estimated corresponding carrier densities.

The specific limitations of the methods used, such as neglecting different relaxation channels in the biexponential decay model of the TRPL data, are beyond the scope of this paper. However, the trends observed with increasing LED active region thickness and increased injection are fully consistent. Overall, the TRPL data also point out the higher efficiency in thinner (3 nm) DH LEDs, and suggest that increasing the number of 3 nm active regions separated by thin and low barriers would help enhance EQE while maintaining high IQE by increasing the radiating volume.

IV. CONCLUSIONS

Bearing efficiency loss/retention arguments at high current levels in mind, we investigated the quantum efficiencies of DH LED structures with different active region designs. DH LEDs with 3 nm-thick active regions reached very high IQE (97%) at 10^{18} cm^{-3} carrier density and exhibited negligible efficiency droop with increasing injection. Increasing DH thickness from 3 to 6 nm resulted in a decrease in IQE; however, the peak EQE increased, although the rate of increase in EQE with injection slowed down slightly. Further increase of the DH active region thickness to 9 nm improved EQE only at very high injection levels, while 11 nm thick DH showed significantly lower EQE due to relaxation and the degradation of the InGaN material. To increase EQE while maintaining high IQE multiple 3 nm-thick DH active regions separated by 3 nm thick In$_{0.06}$Ga$_{0.94}$N barriers were employed. The dual 3 and 6 nm DH structures were found to be superior to the single DH structures considering both IQE and EQE results comprehensively. In dual 3 nm DH LEDs, the IQE reached above 95% and the EQE doubled compared to the single 3 nm DH LED. Both single and dual 3 nm DH LEDs exhibited negligible droop up to current densities above 500 A/cm^2. Furthermore, LEDs incorporating quad 3 nm DH active regions were observed to improve the

emission further with slight reduction when six DH active regions were employed (hex 3 nm DH). Similarly, by incorporating two 6 nm DH active regions separated by a 3 nm $In_{0.06}Ga_{0.94}N$ barrier into a single LED, the highest peak EQE values were achieved: 12% and 19% higher than those provided by 6 nm DH and 9 nm DH, respectively. Moreover, both the single and dual 6 nm DH LEDs showed similar IQE values, implying that the layer quality does not degrade with the inclusion of a second 6 nm DH active region, unlike the significant degradation observed when a single 11 nm-thick DH was used.

Numerical simulations of band structures and radiative recombination are in agreement with experimental results, suggesting better electron hole wavefunction overlap, i.e., high radiative efficiency for thinner active regions and dual DH structures and a general trend of increased overlap with increased injection level. Excitation power intensity dependent TRPL measurements revealed larger radiative recombination rates at higher excitation levels, consistent with simulations. The larger polarization field effects within the thicker DH active regions must be taken into consideration since the electron and hole wavefunction overlap will be reduced considerably, resulting in a slower increase in the quantum efficiency with injection and lower radiative recombination rate. The data in aggregate suggest that the dual or more DH active regions substituting a single layer thick DH active region should be employed for optimum LED designs for high IQE and high EQE with negligible droop, which has its origins in electron leakage and degradation of material quality. Further efforts should be focused on enhancing hole concentration and hole injection efficiency to mitigate or completely eliminate, if possible, the efficiency droop at higher injection levels for the multi-DH active region LEDs.

ACKNOWLEDGMENTS

[1]H. Morkoç, *Handbook of Nitride Semiconductors and Devices* (Wiley-VCH, 2008), Vol. 3, Chap. 1.

[2]Ü. Özgür, H. Liu, X. Li, X. Ni, and H. Morkoç, Proc. IEEE **98**, 1180 (2010).

[3]A. David, M. J. Grundmann, J. F. Kaeding, N. F. Gardner, T. G. Mihopoulos, and M. R. Krames, Appl. Phys. Lett. **92**, 053502 (2008).

[4]J. P. Liu, J. H. Ryou, R. D. Dupuis, J. Han, G. D. Shen, and H. B. Wang, Appl. Phys. Lett. **93**, 021102 (2008).

[5]J. H. Zhu, S. M. Zhang, H. Wang, D. G. Zhao, J. J. Zhu, Z. S. Liu, D. S. Jiang, Y. X. Qiu, and H. Yang, J. Appl. Phys. **109**, 093117 (2011).

[6]N. F. Gardner, G. O. Müller, Y. C. Shen, G. Chen, S. Watanabe, W. Götz, and M. R. Krames, Appl. Phys. Lett. **91**, 243506 (2007).

[7]X. Li, F. Zhang, S. Okur, V. Avrutin, S. J. Liu, Ü. Özgür, H. Morkoç, S. M. Hong, S. H. Yen, T. S. Hsu, and A. Matulionis, Phys. Status Solidi A **208**, 2907 (2011).

[8]M. J. Lai, L. B. Chang, R. M. Lin, and C. S. Huang, Appl. Phys. Express **3**, 072102 (2010).

[9]P. Blood, IEEE J. Quantum Electron **36**, 354 (2000).

[10]V. I. Litvinov, J. Appl. Phys. **88**, 5814 (2000).

[11]R. J. Radtke, U. Waghmare, H. Ehrenreich, and C. H. Grein, Appl. Phys. Lett. **73**, 2087 (1998).

[12]A. Dmitriev and A. Oruzheinikov, J. Appl. Phys. **86**, 3421 (1999).

[13]F. D. Sala, A. D. Carlo, P. Lugli, F. Bernardini, V. Fiorentini, R. Scholz, and J. M. Jancu, Appl. Phys. Lett.**74**, 2002 (1999).

[14]L. Wang, C. Liu, J. N. Lu, L. Liu, N. Y. Liu, Y. J. Chen, Y. F. Zhang, E. D. Gu, and X. D. Hu, Opt. Express **19**, 14182 (2011).

[15]Q. Dai, M. F. Schubert, M. H. Kim, J. K. Kim, E. F. Schubert, D. D. Koleske, M. H. Crawford, S. R. Lee, A. J. Fischer, G. Thaler, and M. A. Banas, Appl. Phys. Lett. **94**, 111109 (2009).

[16]M. H. Kim, M. F. Schubert, Q. Dai, J. K. Kim, E. F. Schubert, J. Piprek, and Y. Park, Appl. Phys. Lett. **91**, 183507 (2007).

[17]X. Ni, Q. Fan, R. Shimada, Ü. Özgür, and H. Morkoç, Appl. Phys. Lett. **93**, 171113 (2008).

[18]J. S. Im, H. Kollmer, J. Off, A. Sohmer, F. Sholz, and A. Hangleiter, Mater. Res. Soc. Symp. Proc. **482**, 513 (1997).

[19]P. Perlin, C. Kisielowski, V. Iota, B. A. Weinsten, L. Mattos, N.A. Shapiro, J. Kruger, E. R. Weber, and J. Yang, Appl. Phys. Lett. **73**, 2778 (1998).

[20]O. Ambacher, J. Majewski, C. Miskys, A. Link, M. Hermann, M. Eickhoff, M. Stutzmann, F. Bernardini, V. Fiorentini, V. Tilak, B. Schaff, and L. F. Eastman, J. Phys.: Condens. Matter **14**, 3399 (2002).

[21]C. K. Sun, S. Keller, G. Wang, M. S. Minsky, J. E. Bowers, and S. P. DenBaars, Appl. Phys. Lett. **69**, 13 (1996).

[22]T. Riemann, J. Christen, H. Teisseyre, P. Valvin, P. Lefebvre, P. Perlin, M. Leszczyñski, and I. Grzegory, J. Appl. Phys. **97**, 103507 (2005).

[23]G. Mohs, B. Fluegel, H. Giessen, H. Tajalli, N. Peyghambarian, P.-C. Chiu, B. S. Phillips, and M. Osin'ski, Appl. Phys. Lett. **67**, 11 (1995).

[24]S.-W. Feng, Y.-C. Cheng, Y.-Y. Chung, C. C. Yang, M.-H. Mao, Y.-S. Linand K.-J. Ma, and J.-I. Chyi, Appl. Phys. Lett. **80**, 4375 (2002).

[25]M. Furis, F. Chen, A. N. Cartwright, H. Wu, and W. J. Schaff, Mater. Res. Soc. Symp. Proc. **743**, art. no. L11.14 (2002).

[26]H. Kim, D.-S. Shin, H.-Y. Ryu, and J.-I. Shim, Jpn. J. Appl. Phys. **49**, 112402 (2010).

[27]C. K. Sun, S. Keller, G. Wang, M. S. Minsky, J. E. Bowers, and S. P. DenBaars, Appl. Phys. Lett. **69**, 1936 (1996).